Available online at www.sciencedirect.com
ScienceDirect
Separation and Purification Technology 62 (2008) 22–31
Separation Purification Technology
www.elsevier.com/locate/seppur

Optimization of PSA process for producing enriched hydrogen from plasma reactor gas

Qinglin Huang, Amir Malekian, Mladen Eić *

Department of Chemical Engineering, University of New Brunswick, P.O. Box 4400, Fredericton, N.B., Canada E3B 5A3

Received 22 May 2007; received in revised form 12 December 2007; accepted 28 December 2007

Abstract

Hydrogen purification with optimum recovery and energy consumption from various process streams represents one of the major commercial uses of pressure swing adsorption (PSA) technology. In the plasma process for hydrogen production, the effluent stream from a reactor has to be processed to obtain the high purity hydrogen before being fed to fuel cells for power generation or stored in tanks. The major impurity in the effluent stream is unreacted methane.

A rigorous PSA model for simulation and optimization purposes has been developed. The non-isothermal, bulk separation with variable superficial velocity and dispersion coefficient, linear driving force approximation for particle uptake, and Langmuir isotherm to represent adsorption equilibrium were applied in the PSA modeling. The model was solved using gPROMS software. The extensive simulation results involving parametric studies of PSA separation performance were well matched with the experimental results using an activated carbon made from coconut shell as an adsorbent. The optimal conditions for separation of 50%H_2/50%CH_4 mixture in a laboratory-scale PSA unit, and separation of 25%H_2/75%CH_4 mixture, representing exit gas from plasma reactor, in a pilot-scale PSA unit were obtained by carrying out optimization routines in gPROMS.

Keywords: PSA; Purification; Hydrogen and methane; Adsorption; Optimization; gPROMS; Plasma process

1. Introduction

Recent developments in the fuel cell industry have increased the demand for the supply of pure hydrogen. One of the novel processes to produce hydrogen is the plasma process, which is considered to be a part of new generation technologies, since it does not produce carbon dioxide as a side product [1,2]. However, hydrogen in the product gas stream has to be separated from other gases before being compressed to high pressures and effectively used in fuel cells or other devices for power generation, transportation, and other applications. The effluent gas stream from the plasma reactor contains mainly hydrogen and methane, as well as other minor impurities, such as light hydrocarbons.

Pressure swing adsorption (PSA) is a mature technology that is widely used for hydrogen purification and separation from different process streams [3]. A number of studies dealing with PSA processes for hydrogen separation and purification from impurities, such as CH_4 and CO_2, have been published [4–10]. However, only a limited number of them [9,10] reported the optimization of PSA separation process for hydrogen production. The optimization work is necessary for PSA system due to the complicated nature of cyclic process, and the fact that there is a large number of design parameters such as step times, pressure, temperature, gas velocity and bed dimensions, which can affect PSA separation performance. For that reason, it is not always feasible to carry out a large number of PSA experiments to define the optimum conditions. So far there has been a number of studies investigating the optimization of various PSA processes [9–14]. Among them, Biegler and coworkers [9,10,13,14] performed comprehensive theoretical studies on single-bed and multi-bed PSA optimization. They used different mathematical and computational strategies to achieve more accurate cyclic steady states, better convergence, faster and more efficient computation. However, none of the previous studies involved both experimental measurements and theoretical PSA simulation and optimization for the comparisons.

The objective of this work was to optimize single-bed PSA process to separate hydrogen from other constituents comprising

* Corresponding author. Tel.: +1 506 453 4689; fax: +1 506 453 3591.
E-mail address: meic@unb.ca (M. Eić).

1383-5866/$ – see front matter © 2008 Elsevier B.V. All rights reserved.
doi:10.1016/j.seppur.2007.12.017

output gas stream from the plasma reactor system. The parametric studies on the separation performance of PSA system were also carried out both experimentally and theoretically.

2. PSA model and solution

2.1. Model assumptions

The mathematical model describes a bench-scale, single-bed pressure swing adsorption system that undergoes four-step cycles such as pressurization with hydrogen product or feed mixture, adsorption, depressurization and regeneration. The following assumptions have been considered in the model development:

(i) The ideal gas law.
(ii) The frictional pressure drop through the adsorption bed is negligible, which is valid for a small-scale PSA experimental system.
(iii) The flow pattern is described by an axially dispersed plug flow model.
(iv) The adsorption equilibrium is represented by the extended Langmuir isotherm for binary mixture.
(v) There are no radial variations in temperature, pressure, concentration or velocity.
(vi) Transport and physical properties are temperature independent.
(vii) Bed pressure is constant during the adsorption and regeneration steps; and in the pressurization and depressurization steps, the bed pressure follows a linear dynamic differential equation of the following form [3]:

$$\frac{\mathrm{d}P}{\mathrm{d}t} = -a_i(P - P_\mathrm{k}) \tag{1}$$

where t is time, P is bed pressure, P_k is the end-pressure in the bed during pressurization or depressurization step and the values of a_i are determined by fitting the above equation with experimentally obtained pressure profiles during pressurization and depressurization steps, respectively.
(viii) The adsorption rate is approximated by a linear driving force (LDF).

2.2. Model equations

The component and overall mass balances for the system are represented by Eqs. (2) and (3), respectively [3]. The gas interstitial velocity will change over the length of the bed, as described by Eqs. (3a) and (3b).

$$-D_L\frac{\partial^2 c_i}{\partial z^2} + \frac{\partial c_i}{\partial t} + u\frac{\partial c_i}{\partial z} + c_i\frac{\partial u}{\partial z} + \frac{1-\varepsilon_\mathrm{bed}}{\varepsilon_\mathrm{bed}}\frac{\partial q_i}{\partial t} = 0 \tag{2}$$

For constant pressure steps during adsorption and regeneration:

$$C\frac{\partial u}{\partial z} + \frac{1-\varepsilon_\mathrm{bed}}{\varepsilon_\mathrm{bed}}\sum_{i=1}^{n}\frac{\partial q_i}{\partial t} = 0 \tag{3a}$$

For variable pressure steps during pressurization and depressurization:

$$C\frac{\partial u}{\partial z} + \frac{\partial C}{\partial t} + \frac{1-\varepsilon_\mathrm{bed}}{\varepsilon_\mathrm{bed}}\sum_{i=1}^{n}\frac{\partial q_i}{\partial t} = 0 \tag{3b}$$

where u is the gas interstitial velocity, c_i is the gas phase concentration of component i, C is the gas phase total concentration ($=P/R_\mathrm{g}T$), R_g is the ideal gas constant, T is the temperature, z is the axial co-ordinate, q_i is the adsorbed phase concentration of component i; ε_bed is the bed voidage and D_L is the axial dispersion coefficient, which can be estimated by the following equation [15]:

$$D_L = 0.7\,D_\mathrm{m} + \frac{1}{2}\mathrm{d_p}u \tag{4}$$

where d_p is the diameter of adsorbent particle, D_m is the molecular diffusivity, which can be calculated from the well-known Chapman–Enskog equation.

Since heat effects are significant due to the high concentration of sorbate species, e.g., methane, the energy balance is coupled to the mass balance to fully describe the system:

$$(\varepsilon_t\rho_\mathrm{gas}C_\mathrm{pg} + \rho_\mathrm{bed}C_\mathrm{ps})\frac{\partial T}{\partial t} + \rho_\mathrm{gas}C_\mathrm{pg}\varepsilon_\mathrm{bed}u\frac{\partial T}{\partial z} - K_L\frac{\partial^2 T}{\partial z^2} - \rho_\mathrm{bed}\sum_{i=1}^{n}\Delta H_i\frac{\partial q_i}{\partial t} + \frac{2h}{R_\mathrm{bed}}(T - T_\mathrm{wall}) = 0 \tag{5}$$

where C_pg and C_ps are the gas and solid particle heat capacities, respectively, ρ_bed and ρ_gas are bed and bulk gas densities, respectively, h is the heat transfer coefficient, K_L is the thermal dispersion coefficient, R_bed is the column radius, T_wall is the column wall temperature, ΔH_i is the isosteric heat of adsorption, which is obtained from the Clausius-Clapeyron equation at the constant loading:

$$\left[\frac{\mathrm{d}\ln P_i}{\mathrm{d}(1/T)}\right]_q = -\frac{\Delta H_i}{R_\mathrm{g}} \tag{6}$$

The consistency of PSA model largely depends on the adequacy of model assumptions and the related information used in the model, e.g., equilibrium isotherm and mass transfer models. In this work, the adsorption rate is represented by the LDF model:

$$\frac{\partial q_i}{\partial t} = k_i(q_i^* - q_i) \tag{7}$$

where k_i is the LDF mass transfer coefficient, q_i^* is the equilibrium loading of component i at time t. For binary adsorption equilibrium behavior, the following forms of extended Langmuir isotherm are used to determine q_i^* for the PSA mathematical model:

$$q_i^* = \frac{K_i c_i}{1 + \sum_{i=1}^{n} b_i c_i} \tag{8}$$

$$\text{where} \quad K_i = K_{1,i}\mathrm{e}^{(K_{2,i}T)} \quad \text{and} \quad b_i = b_{1,i}\mathrm{e}^{(b_{2,i}T)} \tag{9}$$

where b_i is the single component equilibrium constant, K_i is the Henry's constant, $K_{1,i}$, $K_{2,i}$, $b_{1,i}$ and $b_{2,i}$ are the temperature independent parameters.

Table 1
Boundary conditions of PSA process

Pressurization with feed mixture	Pressurization with product hydrogen	Adsorption	Depressurization	Regeneration
$c_i\|_{z=0} = c_{f,i}$	$\left.\frac{\partial c_i}{\partial z}\right\|_{z=0} = 0$	$c_i\|_{z=0} = c_{f,i}$	$\left.\frac{\partial c_i}{\partial z}\right\|_{z=0} = 0$	$\left.\frac{\partial c_i}{\partial z}\right\|_{z=0} = 0$
$\left.\frac{\partial c_i}{\partial z}\right\|_{z=L} = 0$	$c_i\|_{z=L} = c_{\text{product},i}$	$\left.\frac{\partial c_i}{\partial z}\right\|_{z=L} = 0$	$\left.\frac{\partial c_i}{\partial z}\right\|_{z=L} = 0$	$c_i\|_{z=L} = c_{\text{product},i}$
$u\|_{z=L} = 0$	$u\|_{z=L} = 0$	$u\|_{z=0} = u_{\text{feed}}$	$\left.\frac{\partial u}{\partial z}\right\|_{z=0} = 0$	$\left.\frac{\partial u}{\partial z}\right\|_{z=0} = 0$
$\left.\frac{\partial u}{\partial z}\right\|_{z=L} = 0$	$\left.\frac{\partial u}{\partial z}\right\|_{z=L} = 0$	$\left.\frac{\partial u}{\partial z}\right\|_{z=L} = 0$	$u\|_{z=L} = 0$	$u\|_{z=L} = u_{\text{purge}}$
$\left.\frac{\partial T}{\partial z}\right\|_{z=L} = 0$	$\left.\frac{\partial T}{\partial z}\right\|_{z=0} = 0$	$T\|_{z=0} = T_{\text{feed}}$	$\left.\frac{\partial T}{\partial z}\right\|_{z=0} = 0$	$\left.\frac{\partial T}{\partial z}\right\|_{z=0} = 0$
$T\|_{z=0} = T_{\text{feed}}$	$T\|_{z=L} = T_{\text{feed}}$	$\left.\frac{\partial T}{\partial z}\right\|_{z=L} = 0$	$\left.\frac{\partial T}{\partial z}\right\|_{z=L} = 0$	$T\|_{z=L} = T_{\text{feed}}$

All boundary conditions for the four steps with respect to the differential variables within the model such as partial concentration, velocity and temperature are summarized in Table 1. Table 2 describes the mole flux into and out of the bed during each of the four steps in the cycle [13]. The differential variables determine the number of moles over the entire cycle, and they are used to determine the performance variables including purity, recovery and power required for the separation described as follows:

$$\text{Purity}_{H_2} = \frac{\int_0^{t_A} (u\, c_{H_2})|_{z=L}\, dt}{\int_0^{t_A} (u\, c_{H_2} + u\, c_{CH_4})|_{z=L}\, dt} \quad (10)$$

For column pressurized with feed mixture,

$$\text{Recovery}_{H_2} = \frac{\int_0^{t_A} (u\, c_{H_2})|_{z=L}\, dt - \int_0^{t_{Pu}} (u\, c_{H_2})|_{z=L}\, dt}{\int_0^{t_P} (u\, c_{H_2})|_{z=0}\, dt + \int_0^{t_A} (u\, c_{H_2})|_{z=0}\, dt} \quad (11a)$$

For column pressurized with hydrogen product,

$$\text{Recovery}_{H_2} = \frac{\int_0^{t_A} (u\, c_{H_2})|_{z=L}\, dt - \int_0^{t_P} (u\, c_{H_2})|_{z=L}\, dt - \int_0^{t_{Pu}} (u\, c_{H_2})|_{z=L}\, dt}{\int_0^{t_A} (u\, c_{H_2})|_{z=0}\, dt} \quad (11b)$$

where t_A, t_P and t_{Pu} are the adsorption, pressurization, and purging (regeneration) times, respectively.

$$\text{Power} = \frac{\gamma}{\gamma - 1} R_g T_{\text{feed}} \left[\left(\frac{P_{\text{feed}}}{P_{\text{atm}}} \right)^{(\gamma-1)/\gamma} - 1 \right] \pi R_{\text{bed}}^2 u_{\text{feed}} c_{\text{feed}} \quad (12)$$

where γ is the ratio of the heat capacities (C_p/C_v).

2.3. Solution methodology

The partial differential equations at the axial dimension are discretized using the centered finite difference method (CFDM). The dynamic simulation is carried out by a scientific package called gPROMS. gPROMS is able to simulate periodic or cyclic processes by adjusting the boundary conditions and keeping the rest of the mathematical formulation unchanged. The dynamic optimizer in gPROMS can optimize the decision variables (bed dimensions) and the operating conditions (bed pressures, flow rates, etc.) simultaneously.

Table 3
Equilibrium parameters for hydrogen and methane in AC(2) sample

Sorbate	$K_{1,i}$ (−)	$K_{2,i}$ (1/K)	$b_{1,i}$ (cm^3/mmol)	$b_{2,i}$ (1/K)
H_2	23.59	−0.010	4.53	−0.010
CH_4	8425.00	−0.018	1617.00	−0.018

3. Experimental

The single component adsorption isotherms of methane and hydrogen at different temperatures were measured using a constant volumetric apparatus [16,17]. To determine a suitable adsorbent for methane–hydrogen separation, two different activated carbon samples and one zeolite 5A sample were tested for this study. The activated carbon samples were provided by Calgon Co. and Barnebey Sutcliffe Co. The Calgon sample was made from coal and labelled as AC (1), while the Barnebey Sutcliffe sample was made from coconut shell and labelled as AC (2). The molecular sieve 5A sample was provided by Union Carbide, Linde division. From the tests carried out in our lab AC (2) was found to have the highest selectivity and optimum adsorption capacity for methane [17] and for that reason was chosen as the adsorbent for the PSA process investigated in this study. Table 3 summarizes the equilibrium parameters, i.e., $K_{1,i}$, $K_{2,i}$, $b_{1,i}$ and $b_{2,i}$, of Eq. (9), for methane and hydrogen for the chosen adsorbent—AC(2).

The PSA experimental studies were performed in a laboratory-scale, one bed, four-step PSA unit designed and

Table 2
Stream variables for PSA cycle

Pressurization with feed mixture	Pressurization with product hydrogen	Adsorption	Depressurization	Regeneration
$\frac{\partial(\text{Feed}_i)}{\partial t} = u c_i\|_{z=0}$	$\frac{\partial(\text{Feed}_i)}{\partial t} = 0$	$\frac{\partial(\text{Feed}_i)}{\partial t} = u c_i\|_{z=0}$	$\frac{\partial(\text{Feed}_i)}{\partial t} = 0$	$\frac{\partial(\text{Feed}_i)}{\partial t} = 0$
$\frac{\partial(\text{Product}_i)}{\partial t} = 0$	$\frac{\partial(\text{Product}_i)}{\partial t} = 0$	$\frac{\partial(\text{Product}_i)}{\partial t} = u c_i\|_{z=L}$	$\frac{\partial(\text{Product}_i)}{\partial t} = 0$	$\frac{\partial(\text{Product}_i)}{\partial t} = 0$
$\frac{\partial(\text{Exhaust}_i)}{\partial t} = 0$	$\frac{\partial(\text{Exhaust}_i)}{\partial t} = 0$	$\frac{\partial(\text{Exhaust}_i)}{\partial t} = 0$	$\frac{\partial(\text{Exhaust}_i)}{\partial t} = -u c_i\|_{z=0}$	$\frac{\partial(\text{Exhaust}_i)}{\partial t} = -u c_i\|_{z=0}$
$\frac{\partial(\text{Purge}_i)}{\partial t} = 0$	$\frac{\partial(\text{Purge}_i)}{\partial t} = -u c_i\|_{z=L}$	$\frac{\partial(\text{Purge}_i)}{\partial t} = 0$	$\frac{\partial(\text{Purge}_i)}{\partial t} = 0$	$\frac{\partial(\text{Purge}_i)}{\partial t} = -u c_i\|_{z=L}$

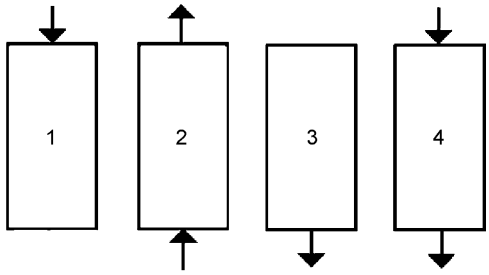

Fig. 1. Four-step PSA cycle: (1) pressurization, (2) adsorption, (3) depressurization, and (4) regeneration.

constructed in our lab [17]. The schematic four-step PSA process is shown in Fig. 1. The experimental system is comprised of a stainless steel column packed with adsorbent, mass flow controllers (Unit Instruments Co., range: 0–10 l/min), and back-pressure regulators (GO Inc., range: 0–250 psig) for pressure control. The column (dimensions listed in Table 4) was kept in a water bath (Cole-Parmer Co., Model: Digital Polystat-temperature controller). The exit gas concentrations from the column were analyzed by a thermal conductivity online analyzer (GOW-MAC Co., Model 20 series), and the output flow rate was measured using a mass flow meter (Unit Instruments Co., range: 0–10 l/min). The details of the experimental set up and procedures were described elsewhere [17]. All PSA experiments were performed for at least 10 cycles to reach cyclic steady state. The column dynamic breakthrough concentration profiles were measured using the same column from the PSA set-up.

4. Results and discussion

4.1. Determination of LDF coefficient and simulation of column dynamics

Since Glueckauf and Coates [18] proposed the important approximation for adsorption system, the LDF model has been widely used as a lumped-parameter model for particle diffusion and adsorption. Malek and Farooq [7,8] analyzed the dynamic breakthrough experiments to study the relationship between LDF coefficient and concentration, pressure, and temperature

Table 4
Properties of adsorbent (AC(2)) and column information

Column	
Bed length	0.3 m
Internal diameter	0.027 m
Physical properties of adsorbent and packing bed	
Packing density	0.427 g/cm^3
Bed voidage	0.404
Particle density	0.716 g/cm^3
Particle radius	2.0×10^{-3} m
Particle porosity	0.6467
Pore diameter	3.0×10^{-9} m
Particle heat capacity (Cps)	1.05 J/g K
Heat transfer coefficient of wall (h)	60 J/m^2 s K

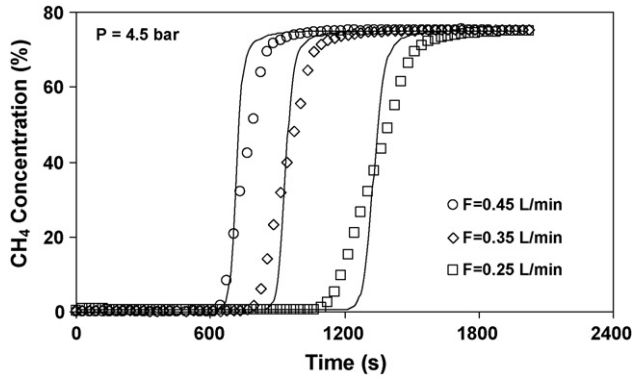

Fig. 2. Concentration breakthrough curves for methane in AC(2) at 303.15 K: bed was initially saturated with hydrogen at 4.5 bar and then purged with 25%H_2/75%CH_4 gas mixture at different flow rates (symbols: experimental results; solid lines: theoretical prediction).

involving a dual-sorbent (activated carbon and silica gel) PSA process. They concluded that the diffusion of light hydrocarbons in activated carbon was controlled by diffusion resistances in meso- and macro-pores, and related the LDF coefficient to the following equation:

$$\frac{1}{k} = \frac{R_p^2}{15\varepsilon_p D_{eff}} \frac{q^* \rho_p}{c_i} \tag{13}$$

where ρ_p is the particle density, R_p is the particle radii, ε_p the is particle voidage, D_{eff} is the effective diffusivity in macro- and mesopores, e.g., combined Knudsen and molecular diffusivities. They found that k value for light hydrocarbons adsorption on various types of activated carbons was nearly inversely proportional to q^*/c_i, and obtained an average D_{eff} value of 0.0085 cm^2/s. This value was shown to be comparable to the values reported in a number of other studies [19–21], where Knudsen and molecular diffusions of light hydrocarbons were also observed to be dominant in activated carbon.

Therefore, Eq. (13) with D_{eff} value of 0.0085 cm^2/s for methane was used for simulation of the bulk PSA separation process. Such approach was verified from the experimental concentration breakthrough results further presented in the following sections.

In this study, breakthrough and desorption experiments of methane in AC(2) were determined under various flow rates and bed pressures. Table 4 provides some relevant data for AC(2). It should be noted that Eqs. (2)–(9), boundary conditions for adsorption step shown in Table 1, and Eq. (13) with D_{eff} value of 0.0085 cm^2/s for methane constitute the theoretical column dynamics model.

Representative comparisons between the measured and predicted breakthrough data are shown in Fig. 2. The simulations showed quantitative agreement with the experimental results, although they were less satisfactory with the decrease of feed flow rate. This may be ascribed to the increasing influence of wall and channel effects at the lower interstitial velocity in the column. Nevertheless, the results proved that Eq. (13) with D_{eff} value of 0.0085 cm^2/s was adequate to estimate the mass transfer coefficient of methane at different operating conditions.

Table 5
Experimental runs used to evaluate effects of various operating parameters on PSA separation performance using AC(2) adsorbent

Run no.	Feed composition	P (bar)	T (K)	Pressurization time (s)	Adsorption time (s)	Blowdown time (s)	Purging time (s)	Adsorption velocity, u (cm/s)	Purging velocity, u (cm/s)	H_2 recovery (%)	Purity (%H_2)
1	50%H_2/50%CH_4	5.8	303.15	225	230	60	360	1.93	−1.93	39.6	99.8
2	40%H_2/60%CH_4	5.8	303.15		230		360	1.93	−1.93	26.0	98.1
3	25%H_2/75%CH_4	5.8	303.15		230		360	1.93	−1.93	12.1	83.7
4	50%H_2/50%CH_4	4.5	303.15		230		360	1.93	−1.93	47.7	88.7
5	50%H_2/50%CH_4	7.2	303.15		230		360	1.93	−1.93	27.8	99.9
6	50%H_2/50%CH_4	8.6	303.15		230		360	1.93	−1.93	25.4	99.9
7	50%H_2/50%CH_4	5.8	303.15		230		360	1.16	−1.16	15.4	99.8
8	50%H_2/50%CH_4	5.8	303.15		230		360	1.56	−1.56	31.0	99.7
9	50%H_2/50%CH_4	5.8	303.15		230		360	2.57	−2.57	41.9	86.8
11	50%H_2/50%CH_4	5.8	303.15		330		360	1.93	−1.93	57.1	81.1
12	50%H_2/50%CH_4	5.8	303.15		430		360	1.93	−1.93	69.8	73.2
13	50%H_2/50%CH_4	5.8	303.15		230		120	1.93	−1.93	72.3	88.9
14	50%H_2/50%CH_4	5.8	303.15		230		240	1.93	−1.93	54.0	96.3
15	50%H_2/50%CH_4	5.8	313.15		230		360	1.93	−1.93	34.3	96.6
16	50%H_2/50%CH_4	5.8	323.15		230		360	1.93	−1.93	35.6	92.6

4.2. Parametric studies

The high purity of product required in this study governed the sequence of the elementary steps. Due to the experimental limitations, the following conditions were considered as basic operating conditions:

- Pressurization with product; feed flow rate: 1.5 L/min; feed composition: 50%CH_4/50%H_2
- Pressure: 5.8 bar; temperature: 303.15 K

From the above operating conditions, the total cycle time was experimentally set at 875 s, where the pressurization time (t_P) was set to 225 s, adsorption time (t_A) to 230 s, depressurization (blowdown) time (t_D) to 60 s and purging (regeneration) time to (t_{Pu}) 360 s. It should be noted that t_P and t_D have little effect on PSA separation performance, and were set to the same values as being used on the existing PSA apparatus, e.g., it took 225/60 s to pressurize/depressurize the system as the inlet/outlet valve was open at a certain extent. The inlet/outlet valve could be adjusted to keep same t_P and t_D for other operating conditions. On the other hand, t_A and t_{Pu} are key factors influencing the PSA separation performance. They were determined from breakthrough and desorption times of methane, when the column exit methane concentration started to increase from 0 and decrease to 0, respectively. In this study, the flow and concentration parameters were considered the main parameters used to determine the performance of the PSA unit. The recovery and product purity, obtained from the PSA model, are compared with the experimental results and presented in the following sections. The experimental data from the PSA runs and the obtained separation performance from parametric study are summarized in Table 5.

4.2.1. Effect of feed composition

Comparisons between experimental results and theoretical prediction for different feed compositions are illustrated in Fig. 3(a). It is clear that PSA model is able to provide good prediction of experimental results under various feed composition. Hydrogen purity decreased slightly as feed methane concentration was increased from 50% to 60%, while it decreased sharply as methane concentration was further increased to 75% or hydrogen concentration decreased to 25%. This is because the selected adsorption time is close to the breakthrough times of the former two runs, where a limited amount of methane breaks through the column. For the latter run, the selected adsorption time is longer than the breakthrough time, resulting in a large amount of methane in the product gas. It was also observed that hydrogen recovery decreased substantially with the increasing feed methane concentration. These suggest that higher methane concentration is unfavorable for PSA separation.

As can be seen from Table 5, hydrogen recovery of 25%H_2/75%CH_4 feed composition is very low (12.1%) due to the experimental limitations [17]. For that reason, 50%H_2/50%CH_4 feed composition was used for further investigation of parameter effects on separation performance of the laboratory-scale PSA system.

4.2.2. Effect of adsorption pressure

The effects of adsorption pressure on the separation performance of the laboratory-scale PSA system were investigated for constant feed and regeneration flow rates as well as same step times. The results for hydrogen recovery and product purity are shown in Fig. 3(b). The simulation and experimental results are in a good agreement. By increasing pressure, the purity increased and approached a constant value. Apparently, there was no advantage to increase pressure beyond 5.8 bar, since no breakthrough of methane was observed. At the low operating pressure, there was either a complete or partial breakthrough of methane, reducing the product purity. The hydrogen recovery decreased gradually with pressure, indicating that higher adsorption pressure is favorable for higher purity, but has the opposite effect on the recovery.

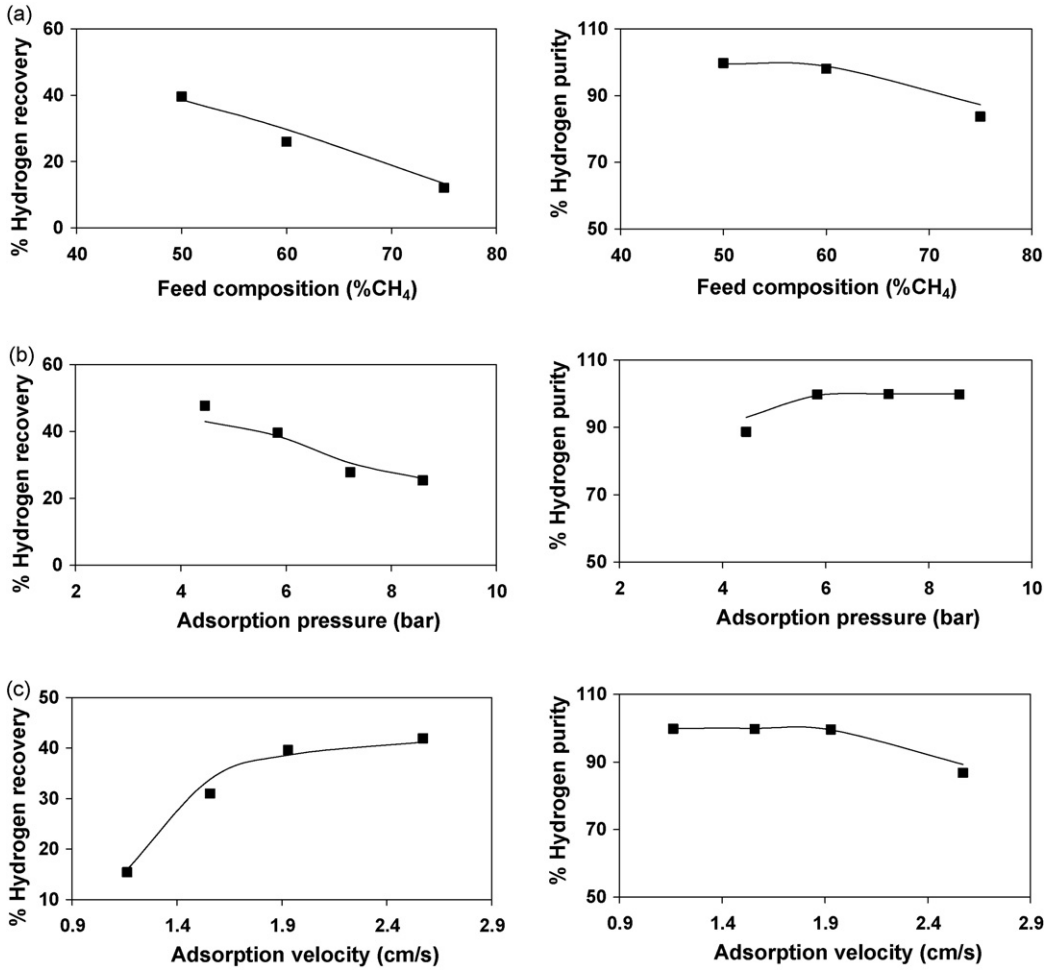

Fig. 3. Effects of (a) feed composition (PSA run no.: 1–3 in Table 5), (b) adsorption pressure (PSA run no.: 1,4–6 in Table 5), and (c) adsorption velocity (PSA run no.: 1,7–9 in Table 5) on PSA separation performance. Symbols: experimental results; solid lines: simulation results.

4.2.3. *Effect of interstitial velocity*

In the commercial PSA system, the interstitial velocity of gas in the column is the other important operating parameter. Fig. 3(c) shows the experimental and simulation results regarding the effects of the interstitial velocity on the separation performance of the PSA system. The quantitative agreement between experimental results and model predictions is considered excellent. The product purity decreased gradually with interstitial velocity (or feed flow rate), while the recovery increased to a larger extent. When the feed flow rate was increased, the breakthrough time of methane decreased; and consequently, with the constant cycle time, this caused a decrease in the product purity. The decrease in purity is dependent on the extent of methane breakthrough. For the lower feed flow rate runs, the breakthrough of methane was insignificant; therefore, the purity only dropped slightly. On the other hand, at higher velocities the methane breakthrough became more significant, causing a rapid drop in purity. The same behavior was reported in the literature [7].

The results reveal that, the maximum recovery and the high product purity can be both obtained at an optimal interstitial velocity of 1.93 cm/s. This simply means that the maximum capacity of the column is utilized when the optimal velocity is reached. In practice, it is possible to obtain very high hydrogen purity and optimal hydrogen recovery by operating at a short adsorption time (cycle time) and a low interstitial velocity.

4.2.4. *Effect of adsorption time*

The summary of the adsorption time effects on product purity and recovery are illustrated in Fig. 4(a). Similarly, the quantitative agreement between experimental and theoretical results is remarkable. The results revealed that increasing the duration of the high-pressure adsorption step had a similar effect on the recovery and purity as increasing the interstitial velocity. Increasing the adsorption step time decreased the purge/feed (P/F) ratio and, consequently, decreased the product purity. The effects of P/F ratio on the purity of the weakly adsorbed component have been reported elsewhere in the literature [8].

4.2.5. *Effect of purging time*

The effect of the purging time on the performance of the PSA process is illustrated in Fig. 4(b). The PSA model showed again to be able to successfully simulate such an effect. The purging time has an opposite effect compared to the adsorption time. An increase in purging time signified more cleaning of the adsorption bed, rendering higher purity and lower product recovery.

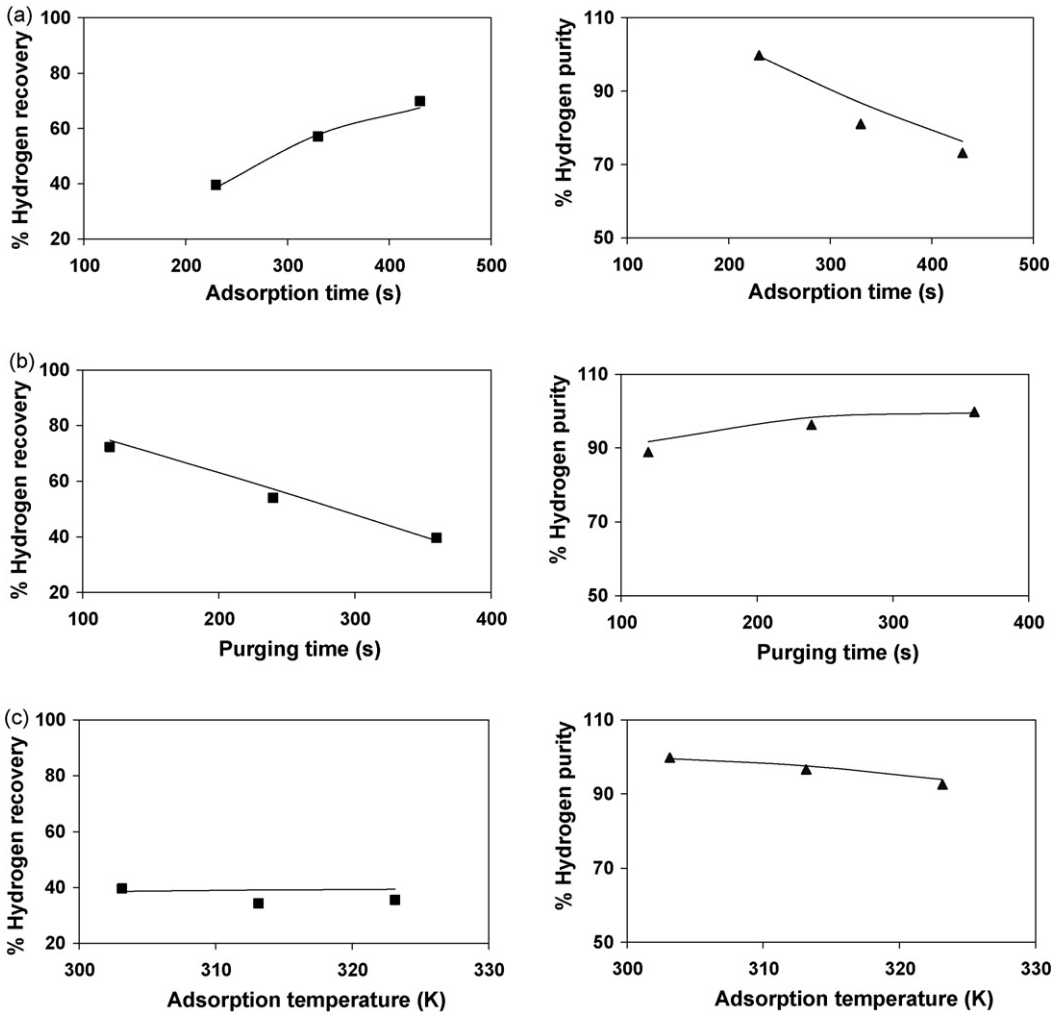

Fig. 4. Effects of (a) adsorption time (PSA run no.: 1,11,12 in Table 5), (b) purging time (PSA run no.: 1,13,14 in Table 5), and (c) adsorption temperature (PSA run no.: 1,15,16 in Table 5) on PSA separation performance. Symbols: experimental results; solid lines: simulation results.

4.2.6. *Effect of temperature*

The effects of the temperature on the performance of the PSA process are plotted in Fig. 4(c). As can be observed, the simulation results are in concurrence with the experimental results. When temperature increased, the purity slightly decreased, while product recovery remained nearly constant. With an increase in the temperature, the adsorption capacity of the adsorbent (activated carbon) for hydrogen and methane decreased, leading to shorter breakthrough time, and hence lower product purity at the constant cycle time.

In summary, the PSA simulation model successfully predicts both hydrogen recovery and purity at various operating conditions. This is particularly important for optimization study, which will be discussed in the following section.

4.3. *PSA optimization*

4.3.1. *Cyclic steady state*

PSA processes are intrinsically dynamic operating in periodic fashion with a fixed cycle time. The performance of a PSA process depends on a number of design and operating parameters. Minimum operating cost, while considering maximum purity or maximum recovery of high purity of product, is particularly important when the PSA process is used as a gas separation system.

Smith and Westerberg [12] investigated the cyclic operating schedule of a PSA system and implemented the mixed-integer nonlinear program to measure the optimal values of the process with respect to the desired operating conditions. Nilchan and Pentelise [22] applied a complete discretization (CD) method that discretized both spatial and time domains for optimization of both traditional PSA and rapid PSA processes. Recently Ko et al. [13,14] investigated the simulation and optimization of a PSA process for CO_2 sequestration. In their model, constant superficial velocity and mass transfer coefficient were considered due to the inherent purification purpose of PSA system. For simulation and optimization, the spatial domain was discretized, which was called single discretization (SD) method. Because of its easier conversion, the SD methodology was considered to be more reliable than the CD method for the optimization of cyclic adsorption processes in the gPROMS modeling system [14].

In order to achieve cyclic steady state (CSS) for the system, the mole fraction and solid concentration bed profiles should be identical at the beginning and at the end of each cycle. The model was first simulated to CSS. Then the resulting bed profiles were discretized by SD method, and fed to gOPT as an initial guess for the optimal CSS condition. As mentioned, gOPT is the dynamic optimizer within the gPROMS program. It allows to specify ranges for the design and operating variables, and optimize over any performance variable and arithmetic combination of performance variables. The following equations are considered to determine CSS for optimization [13]:

$$\left|\left(\int_{0^+}^{L^-}\frac{c_i}{C}\mathrm{d}z\right)_{t=0}-\left(\int_{0^+}^{L^-}\frac{c_i}{C}\mathrm{d}z\right)_{t=t_{\mathrm{cycle}}}\right|\le\delta;$$

$$\left|\left(\int_{0^+}^{L^-}q_i\mathrm{d}z\right)_{t=0}-\left(\int_{0^+}^{L^-}q_i\mathrm{d}z\right)_{t=t_{\mathrm{cycle}}}\right|\le\delta;$$

$$\left.\frac{c_1}{C}\right|_{t=0}+\left.\frac{c_2}{C}\right|_{t=0}=1$$

where δ has a small value of 0.001.

In this work, we first attempted to optimize the operating conditions using 50%H_2/50%CH_4 as feed composition to the current laboratory-scale PSA unit, and then used the similar scheme to obtain optimal conditions for a feed composition of 25%H_2/75%CH_4 coming from the plasma reactor to a pilot-scale PSA unit.

4.3.2. Optimization for 50%H_2/50%CH_4 separation

We considered two optimization cases for 50%H_2/50%CH_4 separation, based on minimum power for higher purity. The constraints of these cases are the same except for their concentration limits. The objective function, for both cases, is minimum power. The constraint regarding the lower bond of the hydrogen purity in the first case was 80% and for the second case was 90%. The following constraints were considered:

$$2\,\mathrm{bar}\le P_{\mathrm{feed}}\le 8\,\mathrm{bar};\quad 10\,\mathrm{s}\le t_{\mathrm{purge}}\le 110\,\mathrm{s};$$

$$0.001\,\mathrm{m/s}\le u_{\mathrm{feed}}\le 0.1\,\mathrm{m/s}$$

$$-0.01\,\mathrm{m/s}\le u_{\mathrm{purg}}\le -0.0001\,\mathrm{m/s};\quad \mathrm{Purity}_{H_2}\ge 80\%\ (\mathrm{case\ 1});$$

$$\mathrm{Purity}_{H_2}\ge 90\%\ (\mathrm{case\ 2})$$

It should be noted that, in order to find the desired optimal conditions, some of the constraints such as pressurization time, adsorption time, depressurization time, and purging pressure, should be kept constant for the computation conversion.

The optimization results are shown in Table 6. Compared with the first case, the second case required higher purity, i.e., the lower bond set to $\mathrm{Purity}_{H_2}\ge 90\%$. The purpose was to determine the effect on recovery and operating (minimum) power. Comparison between the two cases showed that the purging time was increased for higher product purity. Also, the power consumption for the second case was higher than for the first case, due to the higher feed velocity. Furthermore, the recovery involving the second case dropped to 75.5%.

Table 6
Optimization results for separation of 50%H_2/50%CH_4 mixture

Operating conditions	Case 1[a]	Case 2[b]
Feed pressure (bar)	8	8
Adsorption interstitial velocity (cm/s)	1.93	2.03
Regeneration interstitial velocity (cm/s)	−1.93	−1.08
Pressurization time (s)	225	225
Adsorption time (s)	230	230
Depressurization time (s)	60	60
Purging time (s)	27	110
H_2 purity (%)	80	90
H_2 recovery (%)	79.6	75.5
Temperature (K)	303.15	303.15
Power (J/s)	2.63	2.76
Computational time (s)	1292	1231

[a] Case 1: optimization results for minimum power.
[b] Case 2: optimization results for minimum power with higher product purity.

4.3.3. Optimization for 25%H_2/75%CH_4 separation

As discussed above, it was difficult to obtain reasonable separation performance for a feed composition of 25%H_2/75%CH_4, which represents the outlet gas streams of plasma reactor, from the current laboratory-scale PSA unit. Therefore, in this section we seek to investigate the separation of 25%H_2/75%CH_4 from a pilot-scale PSA unit theoretically using gOPT. The pilot-scale PSA column dimension and operating conditions are presented in Table 7. Other physical properties of adsorbent—AC(2) are shown in Table 4.

Here we also simulate each of PSA steps to cyclic steady state. We consider two types of pressurization schemes: the bed is co-currently pressurized with a feed pressure (25%H_2/75%CH_4, denoted as case A), and counter-currently pressurized with product H_2 at ambient temperature (denoted as case B). The operating conditions of the other three steps of PSA are similar. We determined the step times for both cases by running a number of PSA simulations, and chose those settings that were able to generate the desired high product purity. For case A, all four-step times were set to 20 s. For case B, the pressurization and depressurization steps were set to 30 s, while the adsorption and regeneration steps were set to 60 s. The simulation results at CSS, where temperature, mole fraction, and solid concentration bed profiles are

Table 7
Pilot-scale PSA column dimension and operating conditions

Column	
Bed Length (m)	1.0
Internal diameter (m)	0.5
Bed voidage	0.4
Operating conditions	
Gas feed composition	25%H_2/75%CH_4
Adsorption interstitial velocity (m/s)	0.25
Purging interstitial velocity (m/s)	−0.19
Adsorption pressure (bar)	5
Ambient pressure (bar)	1
Temperature (K)	303.15

Table 8
CSS results and dynamic optimization results

CSS simulation results	Case A[a]	Case B[b]
CSS simulation results		
Number of cycles	1000	2000
Hydrogen flow rate (m^3/h)	13.04	1.31
Hydrogen purity (%)	99.97	99.99
Hydrogen recovery (%)	26.14	5.01
Computational time (s)	2720	4923
Dynamic optimization results		
Adsorption pressure (bar)	6	6
Adsorption interstitial velocity (m/s)	0.26	0.24
Purging interstitial velocity (m/s)	−0.21	−0.14
Hydrogen purity (%)	99.85	99.85
Hydrogen recovery (%)	33.40	49.94
Computational time (s)	2248	1204

[a] Co-current pressurization with feed gas (25%H_2/75%CH_4).
[b] Counter-current pressurization with product H_2.

identical at the beginning and at the end of each cycle, are summarized in Table 8, and fed to gOPT as an initial guess at the optimal CSS conditions.

In the above section, we used minimum power as the objective function of optimization. Differently, here we seek to maximize the recovery of fuel-cell grade hydrogen (≥99.85% purity). The optimal solutions determined for the two cases are summarized in Table 8. The optimization approach yielded identical product purities and adsorption pressures. Apparently the product pressurization scheme (case B) shows a much higher hydrogen recovery than case A, indicating that it is a more efficient separation method. The result also provides the theoretical evidence that reasonable recovery of high purity of hydrogen can still be obtained by using a pilot-scale column (in Table 7) for PSA separation of 25%H_2/75%CH_4 mixture.

5. Conclusions

This study has presented a methodology for modeling and optimizing the four-step PSA process that separates hydrogen from methane in a bulk separation fashion.

The activated carbon sample prepared from coconut shell was selected as the adsorbent for this study. A mathematical PSA model with linear driving force adsorption rate was developed, and validated by experimental column dynamic breakthrough results. A laboratory-scale PSA unit was employed to investigate the effects of different operating conditions on hydrogen recovery and purity. The variation of the hydrogen recovery and product purity with feed composition, adsorption pressure, interstitial velocity, adsorption time, purging time and temperature were investigated experimentally and theoretically. The PSA model agreed well with the experimental results obtained from the laboratory-scale PSA unit. Regarding the complexity of the bulk separation model, the agreements, both quantitative and qualitative, are considered excellent.

The optimization routines were carried out to examine the optimal conditions for separation of 50%H_2/50%CH_4 from a laboratory-scale PSA unit, and separation of 25%H_2/75%CH_4 from a pilot-scale PSA unit. The objective functions for optimization were minimum power and maximum recovery of high purity hydrogen, respectively. The optimization results for separation of 50%H_2/50%CH_4 suggested that the minimum required power was affected by the adsorption feed velocity and the feed pressure for a certain product purity. The optimal operation conditions for separation of 25%H_2/75%CH_4 from a pilot-scale PSA unit have been obtained. The result indicates that bed pressurized with product is a better scheme to achieve high recovery and product purity. gPROMS has been proved to be an effective tool for PSA simulation and optimization, which could allow for a relatively quick analysis involving a variety of PSA systems.

References

[1] D.I. Slovetskii, Plasma-chemical processes for the preparation of pure hydrogen, High Energy Chem. 40 (2006) 86–92.
[2] W. Cha, S.H. Lee, W.S. Ju, Y. Baek, Conversion of natural gas to hydrogen and carbon black by plasma and application of plasma black, Symposia—American Chemical Society, Div. Fuel Chem. 49 (2004) 181–183.
[3] D.M. Ruthven, S. Farooq, K.S. Knaebel, Pressure Swing Adsorption, VCH Publishers, 1994.
[4] P.L. Cen, W.N. Chen, R.T. Yang, Bulk gas separation by pressure swing adsorption, Ind. Eng. Chem. Fund. 25 (1986) 758–767.
[5] R.T. Yang, S.J. Doong, Gas separation by pressure swing adsorption—a pore-diffusion model for bulk separation, AIChE J. 31 (1985) 1829–1842.
[6] M. Chalendi, D. Tondeur, F. Rolland, A method to obtain a compact representation of process performances from a numerical simulator: example of pressure swing adsorption for pure hydrogen production, Gas Sep. Purif. 9 (1995) 125–135.
[7] A. Malek, S. Farooq, Study of a six-bed pressure swing adsorption process, AIChE J. 43 (1997) 2509–2523.
[8] A. Malek, S. Farooq, Hydrogen purification from refinery fuel gas by pressure swing adsorption, AIChE J. 44 (1998) 1985–1992.
[9] L. Jiang, V.G. Fox, L.T. Biegler, Simulation and optimal design of multiple-bed pressure swing adsorption systems, AIChE J. 50 (2004) 2904–2917.
[10] S.P. Knaebel, D.H. Ko, L.T. Biegler, Simulation and optimization of a pressure swing adsorption system: recovering hydrogen from methane, Adsorption 11 (Suppl.) (2005) 615–620.
[11] H.M. Kvamsdal, T. Hertzberg, Optimization of PSA systems studies on cyclic steady-state convergence, Comput. Chem. Eng. 21 (1997) 819–832.
[12] O.J. Smith, A.W. Westerberg, The optimal design of pressure swing adsorption systems, Chem. Eng. Sci. 46 (1997) 2967–2976.
[13] D. Ko, R. Siriwardane, L.T. Biegler, Optimization of a pressure-swing adsorption process using zeolite 13× for CO_2 sequestration, Ind. Eng. Chem. Res. 42 (2003) 339–348.
[14] D. Ko, R. Siriwardane, L.T. Biegler, Optimization of pressure swing adsorption and fractionated vacuum pressure swing adsorption processes for CO_2 capture, Ind. Eng. Chem. Res. 44 (2005) 8084–8094.
[15] D.M. Ruthven, Principles of Adsorption and Adsorption Processes, John Wiley and Sons, New York, 1984.
[16] Q. Huang, S.M. Sundaram, S. Farooq, Revisiting transport of gases in the micropores of carbon molecular sieves, Langmuir 19 (2003) 393–405.
[17] A. Malekian, Adsorption Characterization of Novel Nanoporous Materials and Optimization of Bulk PSA Process to Produce H_2 from Plasma Reactor, PhD thesis, University of New Brunswick, 2006.
[18] E. Glueckauf, J.J. Coates, Theory of chromatography. Part IV. The influence of incomplete equilibrium on the front boundary of chromatograms and on the effectiveness of separation, J. Chem. Soc. 50 (1947) 1315–1319.

[19] X. Hu, D.D. Do, Multicomponent adsorption-kinetics of hydrocarbons onto activated carbon—effect of adsorption equilibrium equations, Chem. Eng. Sci. 47 (1992) 1715–1725.
[20] E. Costa, G. Callega, F. Domingo, Adsorption of gaseous hydrocarbons on activated carbon—characteristic kinetic curve, AIChE J. 31 (1985) 982–991.
[21] C.C. Huang, J.R. Fair, Study of the adsorption and desorption of multiple adsorbates in a fixed-bed, AIChE J. 34 (1988) 1861–1877.
[22] S. Nilchan, C.C. Pantelides, On the optimisation of periodic adsorption processes, Adsorption 4 (1998) 113–147.